Signature of nearly icosahedral structures in liquid and supercooled liquid metals and alloys

P. Ganesh and M. Widom
Carnegie Mellon University
Department of Physics
(Dated: November 11, 2004)

A growing body of experiments display indirect evidence of icosahedral structures in supercooled liquid metals. Computer simulations provide more direct evidence but generally rely on approximate interatomic potentials of unproven accuracy. We use first-principles molecular dynamics simulations to generate realistic atomic configurations, providing structural detail not directly available from experiment, based on interatomic forces that are more reliable than conventional simulations. We analyze the data to quantify the degree of local icosahedral and polytetrahedral order. Comparing elemental metals (Cu and Fe, poor glass formers) with alloys (FeB and FeZrB, better glass formers) we find that introduction of a small concentration of large atoms can relieve the frustration of local icosahedral order.

PACS numbers: Valid PACS appear here

I. INTRODUCTION

Turnbull [1–3] established that metallic liquids can be supercooled if heterogeneous nucleation can be reduced or avoided. Frank [4] showed that icosahedral clustering of 12 atoms about a sphere is energetically preferred to crystalline (e.g. FCC, HCP or BCC) packings for the Lennard-Jones (L-J) pair potentials. The icosahedron is favorable because it is made up entirely of four-atom tetrahedra, the densest-packed cluster possible. Local icosahedral order cannot be propagated throughout space without introducing defects. Based on this, Frank hypothesized that the supercooling of liquid metals might be due to frustrated packing of icosahedral clusters.

Following Franck's hypothesis, Hoare [5] found that for L-J clusters ranging between 2 to 64 atoms at least three types of "polytetrahedral" noncrystalline structures exist, with a higher binding energy than HCP or FCC structures with the same number of atoms. Honeycutt and Andersen [6] found the crossover cluster size between icosahedral and crystallographic ordering around a cluster size of 5000 atoms. They also introduced a method to count the number of tetrahedra surrounding an interatomic bond. This number is 5 for local icosahedral order.

Steinhardt, Nelson and Ronchetti [7] introduced the orientational order parameter $\hat{W}_6$ to demonstrate short range icosahedral ordering in a simulated L-J liquid. Jónsson and Anderson [8] observed local five fold symmetry above the glass transition temperature. They also report that at low temperatures, a two component glass containing a minority of large atoms has a cluster of interpenetrating and face-sharing icosahedra throughout the sample.

Many other simulations have been performed on pure elemental metals and metal alloys, using a modified Johnson potential [9], embedded atom potentials [10, 11], the Sutton-Chen (SC) many body potential [12], to name a few. These potentials model the interatomic interactions with varying, and generally uncontrolled, degrees of accuracy. Ab-initio studies on liquid Copper [13–15] and Iron [16] achieve a high degree of realism and accuracy, but have not been analyzed from the perspective of icosahedral ordering.

Undercooling of quasicrystal-forming alloys by electromagnetic levitation [17] suggests that activation energy for formation of quasicrystalline phase nuclei is lower than for crystalline phases. The decrease in activation energy was seen to be more pronounced for the icosahedral phase than for the decagonal phase.

X-ray scattering studies on the deeply undercooled reactive liquid TiZrNi, which has a stable crystalline phase over a wide range of composition, short-range order similar to the liquid and also a metastable quasicrystalline phase, showed correlation between nucleation barrier and a growing icosahedral short range order with decreasing temperature [18].

Neutron scattering studies of deeply undercooled metallic melts [19] observed the characteristic shoulder on the second peak of the structure factor, which has been identified as a signature of icosahedral short range order [20, 21]. The shoulder height increases with decrease in temperature.

A recent XAS experiment on liquid and undercooled liquid Cu by Di Cicco *et al.* [22] isolated the higher order correlation functions. They applied Reverse Monte-Carlo (RMC) refinement [23–25] simultaneously to diffraction and XAS data to construct a model of the disordered system compatible with their experimental data. They analyze the three body angular distribution function N(θ) and also the orientational order parameter $\hat{W}_6$. Their conclusion was that weak local icosahedral order could be observed in their sample. This experiment provided the most direct experimental evidence to-date of the existence of icosahedra in a liquid metal.

Motivated by these results, we explore the structures of liquid and undercooled liquid metals using first principles simulations. First principles calculations achieve the most realistic possible structures, unhindered by the intrinsic inaccuracy of phenomenological potentials and with the ability to accurately capture the chemical nature and distinctions between different elements and alloys. We use the VASP (Vienna Ab-initio Simulation Package [26, 27]) code which solves the quantum mechanical interacting many-body problem using electronic density functional theory. The trade-off for increased accuracy is a decrease in the system sizes we can study, so we can only observe local order, not long range. Also we are limited to short time scales. When we study glassy alloys, we augment our molecular-dynamics simulation with another algorithm called 'Tempering' or 'replica exchange method' (REM) [28, 29] for fast equilibriation at low temperatures.

Our analysis covers methods that have previously been fruitful. We look at the radial distribution function, the three body angular distribution function, which is simply related to the three body correlation function, the $\hat{W}_6$ parameter as discussed above, and the Honeycutt and Andersen bond statistics method [6].

Liquid and supercooled liquid Copper and Iron showed only weak icosahedral order and very little temperature variation. For FeZrB and FeB, we found that FeZrB showed enhanced icosahedral order when supercooled compared to FeB. This could possibly be explained by formation of disclination line defects [20] anchored on the large Zr atoms, which eases the frustration of icosahedral order on the Fe atoms.

Section II describes our first principles molecular dynamics method in greater detail. Then section III discusses our study on copper. Here we introduce the radial distribution function $g(r)$, the $\hat{W}_6$ bond orientational order parameter, the three body angular distribution function $N(\theta)$, and the Honeycutt and Andersen analysis method. Section IV repeats this analysis for the poor-, moderate- and good-glass-forming series Fe, FeB and FeZrB.

II. FIRST PRINCIPLES METHOD

First principles simulation is an incisive, powerful and well-developed tool based on a quantum mechanical treatment of the electrons responsible for interatomic bonding. Since the method is based on fundamental physical laws and properties of atoms, it can be applied to a wide variety of metal alloys and yields the energy and forces computationally without any adjustable free parameters.

Our $ab-initio$ molecular dynamics simulation program, VASP [26, 27], solves the N-body quantum mechanical interacting electron problem using electronic density functional theory, under the Generalised Gradient Approximation (GGA). We use the ultrasoft pseudopotentials [30, 31] (USPP) or projector-augmented wave [32, 33] (PAW) potentials as provided with VASP. Calculation times grow nearly as the third power of the number of atoms, limiting our studies to sample sizes of around a hundred atoms.

In first-principles molecular dynamics, although interatomic forces and energies are calculated quantum mechanically, we still treat the atomic motions classically, using the Born-Oppenheimer approximation. We use Nose dynamics to simulate in the canonical ensemble at fixed mean temperature. The system was well equilibrated before data was considered for analysis. The simulation started with a random configuration, at a temperature high enough to ensure a liquid state, and was allowed to equilibrate at this high temperature. Subsequently, lower temperatures were simulated starting from previous configurations. All calculations were Γ point calculations (a single 'k' point). The simulation was run on a 2.8GHz Intel Xeon processor.

III. RESULTS FOR COPPER

We took N=100 Cu atoms and applied periodic boundary conditions in an orthorhombic cell. Our unequal lattice parameters avoid imposing a characterestic length on the system. The simulations were done at three different temperatures, T=1623K, 1398K and 1313K in order to compare with Di Cicco's experiments [22]. The melting point of copper is 1356K, so samples at 1623K and 1398K are in the liquid regime, while the one at 1313K is undercooled. We used number densities of 0.0740 Å^{-3}, 0.0758 Å^{-3} and 0.0765 Å^{-3} respectively at T=1623K, 1398K and 1313K. These were obtained from a fit of the XRD experimental densities [34] to a straight line versus temperature. Starting from configurations that had been previously equilibrated at slightly different densities, transients of about 250 steps (1fs per step) passed prior to the onset of equilibrium fluctuations of the energy. After the transient, a total of 1500 MD steps were taken at each temperature, for a total simulation time of 1.5ps. The run time was around 240hrs on a 2.8 GHz Intel Xeon processor for each temperature.

A. Two Body Correlation Function

The two body pair correlation function, $g(r)$, is proportional to the density of atoms at a distance r from another atom. We calculate $g(r)$ by forming a histogram of bond lengths which we then smooth out with a gaussian of standard deviation 0.1 Å. Fig 1 shows the $g(r)$ we obtained at the three different temperatures. Our $g(r)$ at T=1623K, compares well with $g(r)$ interpolated from XRD experiments [34]. The heights of the first peak agree closely, as also the peak positions (r=2.50 Å). Results from neutron diffraction experiment [35] are also comparable to our results. Comparisons with the $g(r)$ for Cu at 1500K from the $ab-initio$ MD studies by Hafner *et. al.* [14] and Vanderbilt *et. al.* [13] finds that the heights of their first peak match well with our $g(r)$

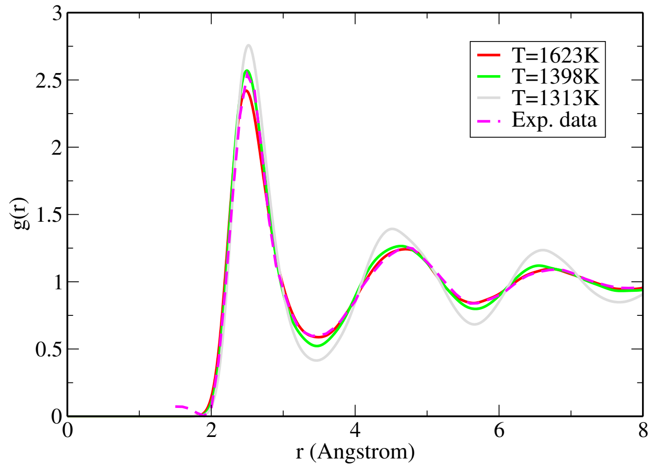

FIG. 1: Simulated liquid Cu correlation function, $g(r)$, at three different temperatures. The simulated curve at T=1623K matches well with the "interpolated" experimental XRD result

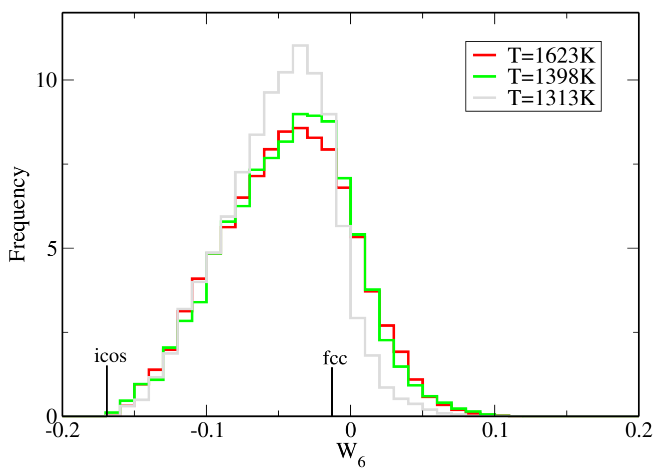

FIG. 2: Simulated $\hat{W}_6$ distributions for liquid Cu. Ideal icosahedron and FCC values are indicated.

TABLE I: $\hat{W}_6$ values for a few clusters

Cluster	HCP	FCC	ICOS	BCC
No. of atoms	12	12	12	14
$\hat{W}_6$	-0.012	-0.013	-0.169	+0.013

(interpolated to T=1500K). But their peak positions are shifted slightly to the left of ours (ours is at 2.50 Å). The $g(r)$ from an embedded-atom method (EAM) model for Cu [11] matches almost exactly with the XRD data at T=1773K.

The growth in height of the first peak, and also the second peak, in the supercooled system at T=1313K suggests an increase of some type of order. However this order is not related to the crystalline FCC equilibrium phase, as we show in the following subsections.

We also ran a separate simulation for N=200 atoms at our highest temperature. We didn't see any significant difference for the two body radial distributions (below 6 Å), the three body angular distributions, or the $\hat{W}_6$ histograms between the N=200 and the N=100 runs. This suggests that N=100 is sufficient for studies of local order of the types we consider here.

B. Bond Orientation Order Parameters

As introduced by Steinhardt *et. al.* [7], the $\hat{W}_l$ parameters are a measure of the local orientational order in liquids and undercooled liquids. To calculate $\hat{W}_l$, the orientations of bonds from an atom to its neighboring atoms are projected onto a basis of spherical harmonics. Rotationally invariant combinations of coeffecients in the spherical harmonics expansion are then averaged over many atoms in an ensemble of configurations. The resulting measures of local orientational order can be used as order parameters to characterise the liquid structures. For an ideal icosahedral cluster, $l = 6$ is the minimum value of l for which $\hat{W}_6 \neq 0$. Table I enumerates $\hat{W}_6$ values for different ideal clusters. We see that the ideal icosahedral value of $\hat{W}_6$ is far from other clusters, making it a good icosahedral order indicator.

We choose a cutoff distance $R_{cut} = 3.4$ Å, near the first minimum of $g(r)$, to specify near neighbors. This value does not change significantly with temperature. With this value of R_{cut} we find an average coordination number of 12.5. Our value of R_{cut} is significantly greater than that of Di Cicco, *et al.*. Our distributions (Fig. 2) show strong asymmetry favoring negative values with tails extending towards the ideal icosahedron value. Because the histogram vanishes as $\hat{W}_6$ approaches its limiting negative value we see that there are essentially no perfectly symmetric undistorted icosahedra present in our simulation. However, a significant fraction do have $\hat{W}_6$ values close to the icosahedral value.

As we lower the temperature, the mean value of $\hat{W}_6$ drops and the peak of the $\hat{W}_6$ distribution shifts to the left. However, the peak never moves below -0.05, and the tail of the distribution at negative $\hat{W}_6$ shows no strong temperature dependence. It seems that there is no change in the number of nearly icosahedral clusters as the temperature drops into the supercooled regime. This may be due to the frustration of packing icosahedra in flat space [36–38]. A perfect 12-fold coordinated icosahedral packing exists in curved three dimensional space, but disclination line defects must be introduced in order to flatten the structure. Disclination line defects cause increased coordination numbers of 14, 15 or 16. Large

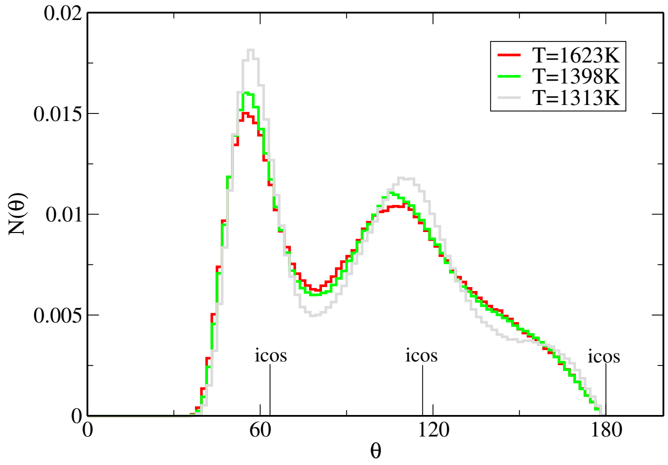

FIG. 3: Distribution of N(θ) for liquid Cu.

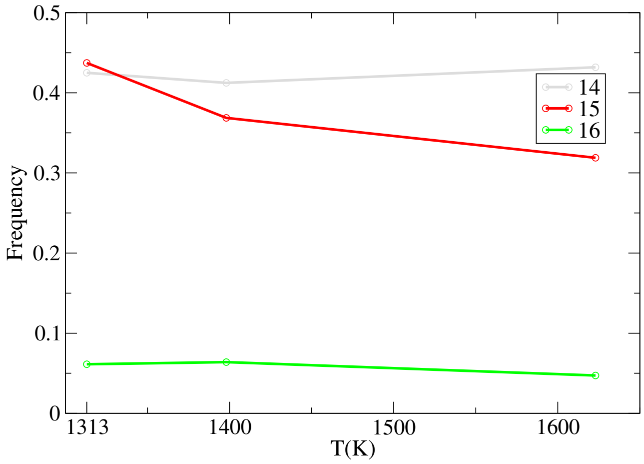

FIG. 4: First two indices of HA analysis for Cu

atoms, if present, would naturally assume high coordination number and aid in the formation of a disclination line network. Our liquid has a single component, so there is no natural way to introduce discilations. This inhibits the growth of a population of atoms with $\hat{W}_6$ close to its ideal icosahedral value.

Comparing our result with that of Di Cicco *et al.* at T=1313K, we see that our curve is more asymmetric towards the negative values than Di Cicco's so that we see a greater fraction of atoms near the ideal icosahedral value of $\hat{W}_6$. The discrepancy probably lies in the difference between the two methods used to generate the positional configurations (the difference is even greater if we use Di Cicco's value of R_{cut}). Their configurations were obtained using reverse monte carlo (RMC), which may not necessarily guarantee the exact positional configurations, while our first principles method should be more accurate in determining these configurations. Of course, Di Cicco's configurations are consistent with experimentally measured three-body correlations. It would be of great interest to see if our configurations are also consistent with the raw experimental data. The differences in $\hat{W}_6$ distributions should not be overstated - the experiment and our simulations both show that liquid and supercooled liquid copper has weak icosahedral order.

C. Bond Angle Distribution N(θ):

The bond angle distribution N(θ) is a simple type of three-body correlation function. Let θ be the angle between bonds from a single atom to two neighbors, and define N(θ) as the probability density for angle θ, normalised such that the total probabilty, $\int N(\theta)d\theta$=1. The distribution, for the central atom of an ideal iosahedron cluster, shows peaks at 63.4, 116.4 and 180.0 degrees. For other crystallographic clusters, like HCP, FCC, and BCC, we see peaks at 60, 90 and 120 degrees. Angles around 60 degrees indicate nearly equilateral triangles that may well belong to tetrahedra.

The distribution for copper at the three temperatures are shown in Fig. 3. The distribution function shows maxima at 56 and 110 degrees with a minimum around 80 degrees. Our curve is similar to that of Di Cicco, but with more pronounced minimum and second maximum. The peak around 60 degrees shows an abundance of nearly equilateral triangles, indicating the presence of tetrahedrons, which can pack to form icosahedra. The minimum close to 90 degrees shows that there aren't many cubic clusters in the undercooled Copper. We also see at the lower temperature, the high-angle tail, turns into a broad maxima, centered at 165 degrees. This maybe because a peak at the exact value of 180 degrees is difficult if we only have distorted icosahedrons. The ordering increases with the lowering of temperature indicating that the number of nearly equilateral triangles increases when the liquid is undercooled, suggesting increase in polytetrahedral order with undercooling. This is consistent with the conclusion we made from the $\hat{W}_6$ order parameter.

D. Honeycutt and Andersen analysis

Honeycutt and Andersen [6] introduced a useful assessment of local structure surrounding interatomic bonds. Local structure around a "root pair" of atoms is classified with four integers (ijkl), with the following set of rules:

(1) The first integer (i) equals 1 if the atoms in the root pair are near neighbors (seperation less than R_{cut}),

and equals 2 if their seperation is less than $2R_{cut}$.

(2) The second integer (j) is the number of near neighbor atoms shared by each atom of the root pair.

(3) The third integer (k) is the number of nearest-neighbor bonds among the shared neighbors.

(4) the fourth integer (l) differentiates between cases when the first three integers are same but the bond geometries are different.

In general, 1421 and 1422 pairs are characterestic of close packed structures (FCC and HCP), 1551 and 2331 pairs are characteristic of a simple icosahedron. Specifically, 1551 indicates a near neighbor bond surrounded by five tetrahedra sharing the bond as a common edge. 2331 indicates a pair of face-sharing tetrahedra. Since we are interested in distinguishing between tetrahedral and crystallographic arangements, we only report the first two indices. Indeed we concentrate on the fraction of "14" and "16" pairs compared to "15" pairs, because these reveal the frustration of icosahedral order.

Fig. 4, shows our results, normalised such that the $1x$ data shows the fraction of bonded pairs. We see that the "15" pairs are quite abundant, though less prevalent than "14". As temperature drops, the "15" fraction grows to match that of "14". The "16's" are very few, and nearly constant with temperature.

Comparing our results with a simulation based on Sutton-Chen potentials [12], we see that their "15" pairs are much higher than their "14" pairs, which are very low, before crystallisation is reached. But in our case, "14" pairs are always higher than all the others, and are fairly constant with temperature. Notice though, that the trends of the "14" and "15" pairs in our graph, suggest a crossover between the two in the supercooled regime. This crossover, due to the sudden increase in the "15" pairs, also possibly explains the dramatic shift of the $\hat{W}_6$ histogram of the supercooled liquid to more negative values. Inspite of the discrepancy between our work and Ref. [12], the relative abundance of "15" and "23" pairs (not shown here), and their trend to increase with supercooling, indicate increase in tetrahedral ordering with supercooling, thereby indirectly supporting nearly icosahedral ordering.

IV. GLASSY ALLOYS

Elemental metals crystallise so easily that they can hardly be made amorphous at any given quench rate. Alloying can improve the ease of glass formation. For some special alloys, a bulk amorphous state can be reached by slow cooling. Pure elemental Fe is a poor glass former, but Fe-based compounds like FeB and especially FeZrB, show improved glass formability.

One reason alloys form glass more easily is that chemical identity introduces a new configurational degree of freedom that evolves slowly. Unfortunately, this makes simulation more difficult. It is especially difficult to equilibrate the system at very low temperatures, because the probability to cross an energy barrier drops, thus forcing the system to be trapped in particular configurations for long times. For this reason we use a Monte-Carlo method, known as tempering or replica exchange [28] to augment our first-principles MD. The method we use is similar to the one in reference [29], except they exchange the potential energy scaling parameter, while we exchange the temperature of the different canonical ensembles. This method allows us to sample the configurational space more efficiently than conventional MD.

TABLE II: Details of Fe and Fe-alloy runs

Chemical Species	Temperatures(K)	density ($\AA^{-3}$)
Fe_{100}	800 and 1833	0.0756
$Fe_{80}B_{20}$	800-1500	0.0814
$Fe_{70}Zr_{10}B_{20}$	800-1800	0.0787

In the canonical ensemble, energy fluctuates at fixed temperature. A given configuration C with energy E can occur at any temperature T with probability $e^{-\beta E}$,($\beta = 1/kT$). Now consider a pair of configurations, C_1 and C_2 of energy E_1 and E_2 occuring in simulations, at temperatures T_1 and T_2. We can take C_1 as a member of the ensemble at T_2, and C_2 as a member of the ensemble at T_1, with a probability

$$P = e^{-(\beta_2-\beta_1)(E_1-E_2)} \tag{1}$$

In practice we perform several MD simulations at temperatures separated by 100K. Every 10 MD steps we compare the configurations at two nearby temperatures and swap them with the above probability. As a result, configurations initially frozen at low temperature can have their temperature to rise. The simulation then can carry the structure over energy barriers after which the temperature can again drop.

To set the densities for our MD simulations, we took a high temperature liquid structure and quenched it, relaxing their positions. Then the density of the relaxed structure was scaled by 6 percent to account for volume expansion, to arrive at the current densities. Notice that we hold the volumes constant independent of temperature because our tempering method requires this. Details regarding the runs at different temperatures and volume, are shown in Table II. For the alloys, each MD step corresponded to 2 fs. About 900 steps were done in total for each temperature in FeB, corresponding to a total time of 1.8ps per temperature, and about 400 steps were done at each temperature for FeZrB, corresponding to 0.8ps per temperature. During this runtime, we saw frequent swapping of configurations at adjacent temperatures, enabling configurations at a lower temperature to spend some time at a higher temperature before they come back to the lower temperature again.

For Pure Fe, we did plain first principles MD, at T=1833K and T=800K, with a 100 atom sample. The densities were taken to be fixed when supercooled. Each MD step corresponded to 1 fs, and the total run time was 2ps.

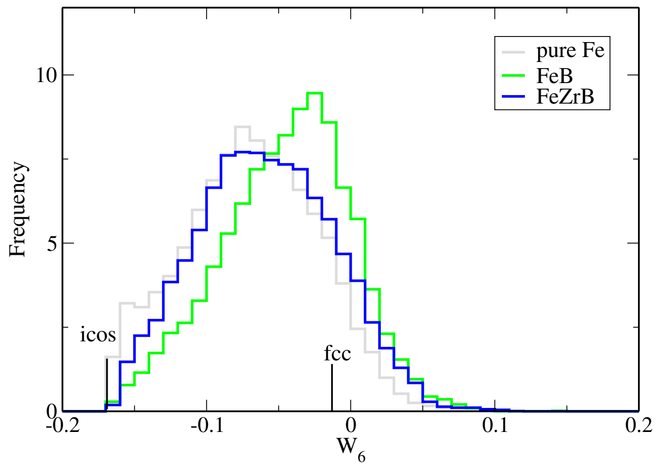

FIG. 5: Distribution of $\hat{W}_6$ around Fe atoms, in supercooled Fe, FeB and FeZrB at T=800K

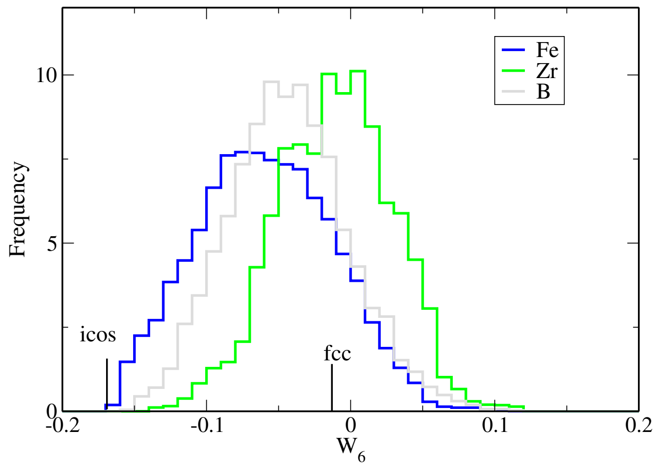

FIG. 6: Distribution of $\hat{W}_6$ for different chemical species in supercooled FeZrB at T=800K

TABLE III: R_{peak}, $g(R_{peak})$ and $R_{min}$for FeZrB at T=800K

chemical pairs	Fe-Fe	Fe-Zr	Fe-B	Zr-Zr	Zr-B	B-B
$R_{peak}(\AA)$	2.57	2.91	2.14	3.44	2.62	1.74
$g(R_{peak})$	2.84	3.13	3.91	1.60	4.01	1.36
$R_{min}(\AA)$	3.45	3.84	2.96	4.18	3.37	2.40

A. Two Body Correlation Function

Table III shows the peak positions, height and the position of the first minima of the different pair correlation functions, in supercooled FeZrB at T=800K. From the heights of the first peak in FeZrB, we see that the strongest bonds form between B and Fe and between B and Zr. Also, the relative bond lengths reveal that B is a small atom, Fe is medium sized and Zr is large. Comparing with simulations of FeB and pure Fe, we find that g_{FeFe} is nearly unaffected by alloying with B or ZrB. Likewise, g_{FeB} and g_{BB} are nearly unaffected by alloying with Zr.

B. Bond Orientation Order Parameter

The $\hat{W}_6$ distributions for Fe, FeB, and FeZrB were explicitly calculated, with the cutoff distances being chosen near the first minima of the partial pair correlation functions (Table: III). The $\hat{W}_6$ distribution for Fe in the three systems at their liquid temperatures (not shown here) resemble each other strongly, and also resemble the curve for liquid Cu at high temperature. Perhaps there is a generic shape for $\hat{W}_6$ distributions in liquid metals at high temperature.

Now compare the Fe based $\hat{W}_6$ distributions for Pure Fe, FeB and FeZrB at their supercooled temperatures in Fig. 5. The FeB distribution is similar to high temperatures, but the FeZrB curve has significantly shifted to the left, extending more towards the ideal icosahedral value of $\hat{W}_6$. The distribution of pure Fe, which is a one component system, does not show any appreciable change from its high temperature curve. One component systems, like pure Fe and pure Cu seem to show similar characterestics of $\hat{W}_6$ when supercooled, due to frustration, which hinders formation of icosahedral clusters.

At temperatures as low as T=800K, the energy of the system is close to the lowest configurational energy of the system, and locally, an icosahedral configuration has the lowest energy. Replacing a few medium sized Fe atoms with smaller B atoms would cause disclination lines to concentrate on Fe, leading to a distortion from ideal icosahedral clustering on these Fe atoms. This causes a reduction in the extreme negative values of $\hat{W}_6$ on Fe atoms in FeB. On the contrary, inclusion of Zr in FeZrB causes disclinations to attach to Zr, easing frustration leading to a more Fe centered clusters with isocahedral ordering. This causes an increase in the negative region of $\hat{W}_6$, as compared to FeB. So it seems that inclusion of the big Zr atom tends to make the local 3D structure around the Fe atoms, more nearly icosahedral. The shift towards the ideal icosahedron value, in the $\hat{W}_6$distribution of FeZrB, suggests that alloying of FeB with the large Zr atom increases icosahedral ordering, thereby reducing its energy.

Fig 6 shows the distribution with centres at Fe, Zr and B, for FeZrB. The histogram with the centre at Zr is almost symmetric about the value of zero. This suggests that the local environment about Zr atoms is nearly spherical, as is expected given its large size. The B centered $\hat{W}_6$ histogram is also assymmetric towards nega-

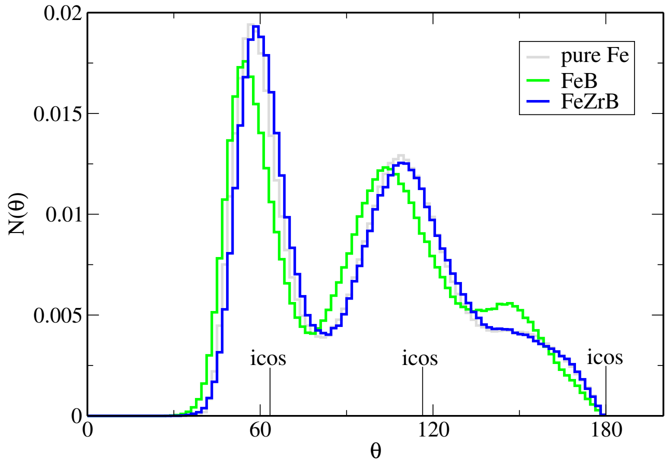

FIG. 7: Distribution of N(θ) for Fe in Pure Fe, FeB and FeZrB at T=800K

tive $\hat{W}_6$ values, and doesn't show any significant change between the two supercooled alloys. Both the B based and Zr based histograms don't show any dramatic change with lowering of temperature or with alloying.

C. Bond-Angle Distribution N(θ)

The three body angular distribution was calculated for the configurations at different temperatures. The cutoff for the calculation of the angular distribution was taken near the first minima of the partial $g(r)$. Fig 7 shows the angular distribution, centered on Fe. In each case, there are sharp peaks around values of 60 degrees and 111 degrees, and a minimum at 90 degrees. The minima at 90 degrees shows that there isn't any cubic order in the system. The peaks at 60, show that there are many nearly equilateral triangles in the configurations. The height at these two peak positions, is more for FeZrB than for FeB at 800K. This again supports the idea of getting more icosahedra by the inclusion of larger Zr atoms. We also notice that these peaks in FeZrB have become higher with supercooling, unlike in FeB. This also supports our conclusion from the $\hat{W}_6$ distribution, that Zr atoms tend to increase icosahedral order on supercooling, easing the process of supercooling of the alloy. That is, it is easier to supercool FeZrB than FeB. The observation, that pure Fe also has the same height as that of FeZrB supports the discination network theory that was put down in the previous subsection. We again see a broad maximum from 150 degrees. This may be due to the fact that an ideal icosahedron also shows a peak at 180 degrees.

The angular distribution of B (not shown here), shows peaks at 70 and 128 degrees with a minima at 97 degrees. The position of the peak heights are shifted by about 7-12 degrees to the right, as compared to the ideal icosahedron peaks. This may be due to the small size of the B atoms, which naturally will tend to increase angles of bonds they form with large atoms. Similarly, peaks on Zr based N(θ) (not shown here) lie around 55 and 96 degrees, about the same values taken by a Friauf polyhedra with a coordination number of 16 [39]

TABLE IV: HA analysis for supercooled FeZrB at T=800K

chemical species	Fe-Fe	Fe-Zr	Fe-B	Zr-Zr	Zr-B	B-B
14 pairs	0.308	0.194	0.55	0.093	0.519	0.727
15 pairs	0.549	0.539	0.392	0.476	0.447	0.181
16 pairs	0.100	0.235	0.006	0.399	0.004	0.000

D. Honeycutt and Andersen analysis

HA statistics show tetrahedral and polytetrahedral ordering. Tetrahedral order supports icosahedral ordering. Since FeZrB showed maximal icosahedral clustering when supercooled, as compared to FeB, we made a HA analysis to the ternary glassy alloys, by looking at pairs of chemical species. The frequency has been normalised such that the $1x$ pairs show the fraction of bonded pairs of that particular chemical species while the $2x$ pairs show the fraction of unbonded pairs for them. Table IV lists the fraction of different $1x$ and $2x$ pairs in supercooled FeZrB.

Among the $1x$ pairs, with Fe as one of the root pairs, the "15"'s are most abundant at all temperatures. They also show a steady enhancement with supercooling, unlike the "14"'s which decrease with supercooling. The percentage of "15"'s for each of the Fe pairs is about the same for the alloys at all temperatures, and exceeds the value for pure Fe at 0800K by 12%. Supercooled pure *Fe* has very few "16"'s (6.3%), about the same as in pure Cu. Adding B to Fe, shows an increase of "16"'s for Fe-Fe pairs to 21%. So additions of a few B atoms, leads to many Z_{16}, Fe centres, making the local geometry about the Fe atoms more spherical. That is why we see the Fe centred $\hat{W}_6$ in FeB shift towards zero. Further inclusion of large Zr atoms to FeB, decreases the "16"'s about the Fe-Fe pairs, easing the frustration off Fe centres. This causes the geometry about Fe centres to be more icosahedral, and hence the shift of the $\hat{W}_6$ towards negative values. Since the fraction of Fe atoms is greater than that of other species, this overall increase in icosahedral order might help in the glass formability of FeZrB.

V. CONCLUSION

This study quantifies icosahedral and polytetrahedral order in supercooled liquid metals and alloys. This is the first such analysis using configurations from first-principles simulations.

While pure elemental liquid Cu and Fe show some tendency to form icosahedra, this tendency is frustrated. Introduction of larger atoms (e.g. Zr in FeZrB) can relieve the frustration leading to strong enhancement in icosahedral order at low temperatures. We suggest, that the formation of icosahedral order and a disclination line network leads to good glass-forming ability in FeZrB.

---

[1] D. Turnbull, J. Appl. Phys. **21**, 1022 (1950).
[2] D. Turnbull, J. Metals **188**, 1144 (1950).
[3] D. Turnbull and R. E. Cech, J. Appl. Phys. **21**, 804 (1950).
[4] F. C. Frank, Proc. R. Soc. London A **215**, 43 (1952).
[5] M. R. Hoare, J. Cryst. Growth **17**, 77 (1972).
[6] J. D. Honeycutt and H. C. Andersen, J. Phys. Chem. **91**, 4950 (1987).
[7] P. J. Steinhardt, D. R. Nelson, and M. Ronchetti, Phys. Rev. B **28**, 784 (1983).
[8] H. Jónsson and H. C. Andersen, Phys. Rev. Lett. **60**, 2295 (1988).
[9] T. Tomida and T. Egami, Phys. Rev. B **52**, 3290 (1995).
[10] C. Kuiying, L. Hongbo, L. Xiaoping, H. Quiyong, and H. Zhuangqi, J. Phys. Condens. Matter **7**, 2379 (1995).
[11] B. Sadigh and G. Grimvall, Phys. Rev. B **54**, 15742 (1996).
[12] H. J. Lee, T. Cagin, W. L. Johnson, and W. A. Goddard, J. Chem. Phys. **119**, 9858 (2003).
[13] A. Pasquarello, K. Laasonen, R. Car, C. Lee, and D. Vanderbilt, Phys. Rev. Letts. **69**, 1982 (1992).
[14] G. Kresse and J. Hafner, Phys. Rev. B **48**, 13115 (1993).
[15] A. A. Valladares, To be published (????).
[16] D. Alfe, G. Kresse, and M. J. Gillan, Phys. Rev. B **61**, 132 (2000).
[17] D. Holland-Moritz, D. M. Herlach, and K. Urban, Phys. Rev. Lett. **71**, 1196 (1993).
[18] K. F. Kelton et al., Phys. Rev. Lett. **90**, 195504 (2003).
[19] T. Schenk, D. Holland-Moritz, V. Simonet, R. Bellisent, and D. M. Herlach, Phys. Rev. Lett. **89**, 075507 (2002).
[20] D. R. Nelson and M. Widom, Nucl. Phys. B **240**, 113 (1984).
[21] S. Sachdev and D. R. Nelson, Phys. Rev. Lett. **53**, 1947 (1984).
[22] A. D. Cicco, A. Trapananti, and S. Faggioni, Phys. Rev. Lett. **91**, 135505 (2003).
[23] R. L. McGreevy, J. Phys. Condens. Matter **13**, R877 (2001).
[24] S. J. Gurman and R. L. McGreevy, J. Phys. Condens. Matter **2**, 9463 (1990).
[25] Y. Wang, K. Lu, and C. Li, Phys. Rev. Lett. **79**, 3664 (1997).
[26] G. Kresse and J. Hafner, Phys. Rev. B **47**, RC558 (1993).
[27] G. Kresse and J. Furthmuller, Phys. Rev. B **54**, 11169 (1996).
[28] R. H. Swendsen and J. S. Wang, Phys. Rev. Lett. **57**, 2607 (1986).
[29] R. Yamamoto and W. Kob, Phys. Rev. E **61**, 5473 (2000).
[30] D. Vanderbilt, Phys. Rev. B **41**, 7892 (1990).
[31] G. Kresse and J. Hafner, J. Phys. Condens. Matter **6**, 8245 (1994).
[32] P. Blochl, Phys. Rev. B **50**, 17953 (1994).
[33] G. Kresse and D. Joubert, Phys. Rev. B **59**, 1758 (1999).
[34] Y. Waseda, The Structure of Non-Crystalline Materials (1980), (McGraw-Hill, New York).
[35] O. J. Eder, E. Erdpresser, B. Kunsch, H. Stiller, and M. Suda, J. Phys. F **10**, 183 (1990).
[36] J. F. Sadoc and R. Mosseri, Phil. Mag. B **45**, 467 (1982).
[37] D. R. Nelson, Phys. Rev. Lett. **50**, 92 (1983).
[38] J. P. Sethna, Phys. Rev. Lett. **51**, 2198 (1983).
[39] J. Hafner, J. Phys. F: Met. Phys. **18**, 153 (1988).